Anatomy and Clinical Examination of the Eye

1

Contents

1.1 Surgical Anatomy of the Retina and Vitreous

1.1.1 The Vitreous

1.1.1.1 Embryology

During early development, the invaginated optic vesicle (optic cup) contains the primary vitreous, a vascularised tissue supplying the lens and retina (both of which have an ectodermal origin). During the third month of gestation, the primary vitreous gradually loses its vascularity and is replaced by the secondary vitreous derived mainly from the anterior retina and ciliary body. The principal remnants of the primary vitreous are Cloquet's canal and some epipapillary gliosis. A mild exaggeration of the latter is seen in Bergmeister's papilla (fibrous tuft) on the optic nerve head, whilst a Mittendorf's dot is a primary vitreous remnant on the posterior capsule of the lens. The hyaloid artery may occasionally persist as a vascular channel growing into the central gel from the optic disc or as a glial plaque on the posterior lens capsule (see Chap. 13).

1.1.1.2 The Anatomy

The vitreous cavity is the space within the eye bounded anteriorly by the lens and its zonular fibres, and more posteriorly by the ciliary body, retina and optic disc. Its volume is usually about 4 ml, though this may increase to as much as 10 ml in highly myopic eyes. Normally, the space is entirely occupied by vitreous gel, a virtually acellular viscous fluid with 99 % water content. Its low molecular and cellular content is essential for the maintenance of transparency. The major molecular constituents of the vitreous gel are hyaluronic acid and type 2 collagen fibrils. The cortical part of the vitreous gel has a higher content of hyaluronic acid and collagen compared with the less dense central gel. In addition, the gel exhibits 'condensations' both within its substance and along its boundaries. The boundary condensations are termed the anterior and posterior hyaloid

T.H. Williamson, *Vitreoretinal Surgery*,
DOI 10.1007/978-3-642-31872-6_1, © Springer-Verlag Berlin Heidelberg 2013

membranes. A central tubular condensation called Cloquet's canal is a remnant of the primary vitreous, stretching sinuously between the lens anteriorly and the optic disc posteriorly. The gel is unimportant in maintaining the shape or structure of the eye. Indeed, apart from its role in oculogenesis, the vitreous has no well-substantiated function. An eye devoid of gel is not adversely affected apart from a poorly understood increased risk of nuclear sclerotic cataract. The pO_2 of the vitreous is relatively low, and it has been suggested that the vitreous may act to reduce oxidative stress on the lens fibres thereby reducing cataractogenesis (Stefansson et al. 1982). The vitreous gel is however primarily implicated in the pathogenesis of a variety of sight-threatening conditions.

1.1.1.3 Anatomical Attachments of the Vitreous to the Surrounding Structures

The posterior hyaloid membrane adheres to the internal limiting membrane of the retina by the insertion of vitreous gel fibrils. The internal limiting membrane has type 4 collagen and is the basement membrane of the Muller cells. The potential space between the internal limiting membrane and the posterior hyaloid membrane is the plane of cleavage of the gel from the retina in posterior vitreous detachment.

The vitreous possesses various sites of increased adhesion to the surrounding structures. These attachments form the basis of much vitreoretinal pathology.

The vitreous base is an annular zone of adhesion some 3–4 mm wide which straddles the ora serrata. Its anterior border is the site of insertion of the anterior hyaloid membrane. The posterior border of the vitreous base is surgically important because this is the anterior limit of potential separation between the gel and the retina and a common site for retinal tear formation. Adhesion of the vitreous base to the retina and the pars plana is difficult to break even with severe trauma.

Weigert's ligament is a circular zone of adhesion, 8–9 mm in diameter, between the gel and the posterior lens capsule. It is the junction between the anterior hyaloid membrane and the expanded anterior portion of Cloquet's canal.

The posterior hyaloid membrane and the slightly expanded posterior limit of Cloquet's canal meet around the margin of the optic disc and produce another ring of adhesion. During posterior vitreous detachment, gliotic tissue is avulsed from the edge of the nerve head to produce the Weiss ring which can be used as an indicator of posterior vitreous detachment (see Fig. 1.1). A circle of relatively increased adhesion to the retina may be present in the parafoveal area and implicated in macular hole formation.

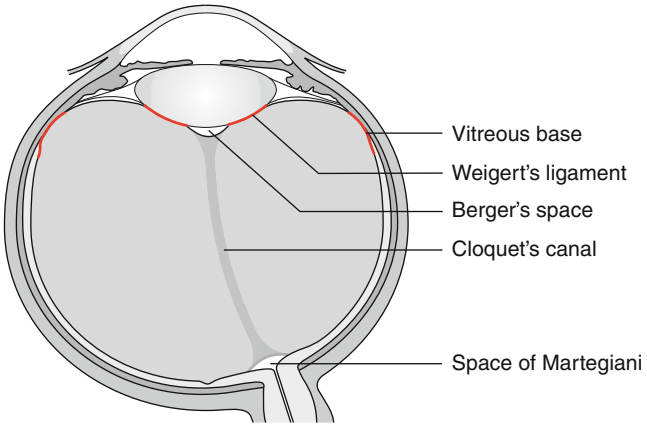

Fig. 1.1 The macroscopic anatomical landmarks are shown

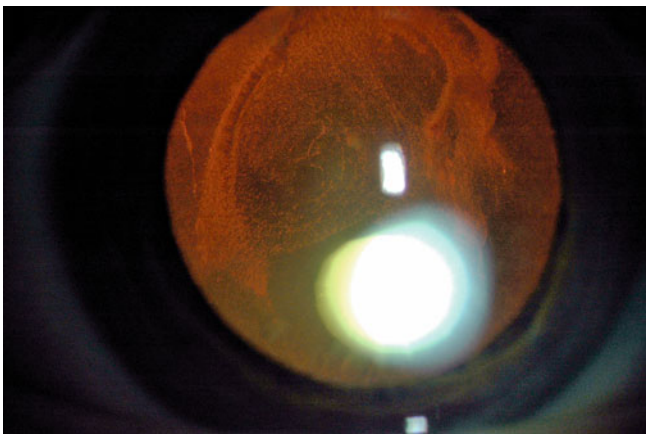

Fig. 1.2 Using retroillumination, Weigert's ligament on the back of the lens can be seen in this patient with mild vitreous haemorrhage

Exaggerated vitreoretinal adhesions are also present in lattice degeneration which comprises oval or elongated areas of thinning and vascular sclerosis in the peripheral retina with overlying degenerative vitreous gel. The lesions are generally orientated circumferentially but may be radially directed along the post-equatorial course of retinal veins. Lattice degeneration is found in approximately 7 % of normal eyes and is frequently associated with tearing of the retina. The surgeon can experience the adhesion of the vitreous to lattice during induced vitreous separation in macular hole surgery (see Chap. 8). Trying to pull the vitreous off lattice will result in tearing of the retina. Some eyes also demonstrate abnormally strong vitreoretinal adhesions along the course of the retinal veins (paravascular adhesions) which may result in retinal tear formation.

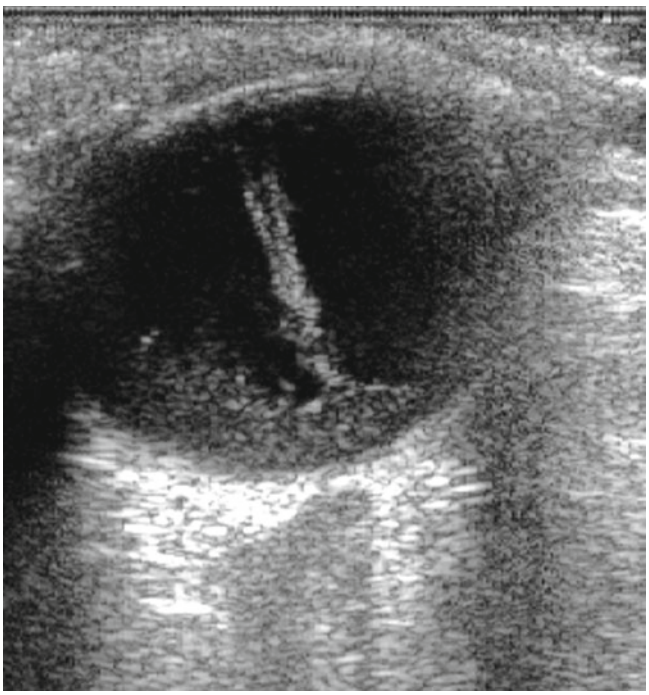

Fig. 1.3 An ultrasound of vitreous haemorrhage (seen especially in the retrohyaloid space) shows Cloquet's canal delineated by the haemorrhage

1.1.2 The Retina

1.1.2.1 Embryology

The optic cup develops from the optic vesicle at 6–7 weeks of gestation and consists of two layers of ectoderm, the outer becoming the retinal pigment epithelium and the inner the neurosensory retina. The space between the two layers is the same as the 'subretinal' space in retinal detachment. The retina develops as two neuroblastic layers, inner and outer, which differentiate into the various cells of the retina. The receptor cells are the last to appear at approximately 13 weeks. At 5.5 months, the adult arrangement can be seen, but the retina is not completely developed until 3–4 months after birth when the macula is formed. The retinal pigment epithelium becomes pigmented from 6 weeks to 3 months of gestation.

1.1.2.2 Anatomy

The retina is divided into regions with the macula consisting of the area between the temporal vascular arcades, serving approximately 20° of visual field. The fovea is the central darkened area with a pit called the foveola. The cones are densest at the fovea, at 15,000/mm^2, with 4,000–5,000/mm^2 in the macula. There are 6 million cones and 120 million rods in total.

Cones provide high-resolution colour vision in photopic conditions. They react quickly and recover rapidly to different light stimuli. Three types of cone photoreceptor exist in the human eye with different opsin proteins bound to a common chromophore (11-*cis*-retinal). The three types provide sensitivities which peak at different light wavelengths: short S cones at 420 nm (blue), middle M cones at 530 nm (green) and long L cones at 560 nm (red).

The retina is organised into four layers of cells and two layers of neuronal connection. The retina has a structural cell called the Muller cell which extends through all the layers. These cells are specialised glial cells which hold a sink of ions during depolarisation of receptors and are essential for the physiology of the eye. They may also have functions in:

- Cone neuroprotection
- Control of vascular permeability and haemostasis
- Pigment recycling

There are astrocytes and microglial cells in addition in the retina.

The retinal layers, from outer to inner retina, are as follows:

Retinal Pigment Epithelium (RPE)

A single layer of pigmented cuboidal epithelial cells which look after the function of the receptors by:

- Absorbing stray light (using melanin pigment)
- Transporting metabolites between the receptors and the choroid
- Providing a blood–retinal barrier
- Regenerating the visual pigments
- Phagocytosing the receptor outer segments leading to lipofuscin production

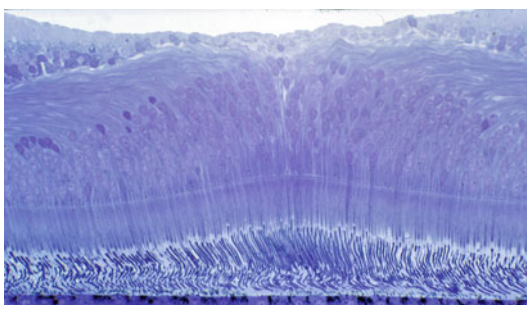

Fig. 1.4 The foveal anatomy showing increased numbers of cones and absence of the nerve fibre layer. (Courtesy of John Marshall)

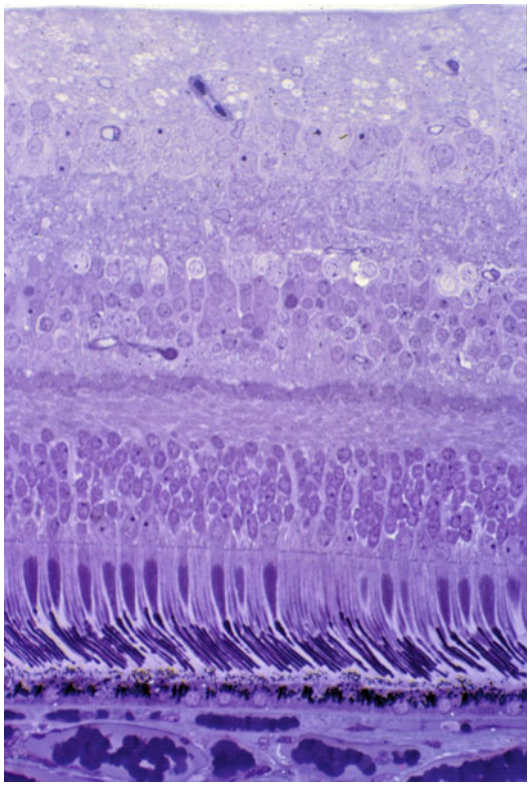

Fig. 1.5 The normal stratified structure of the retina (Courtesy of John Marshall)

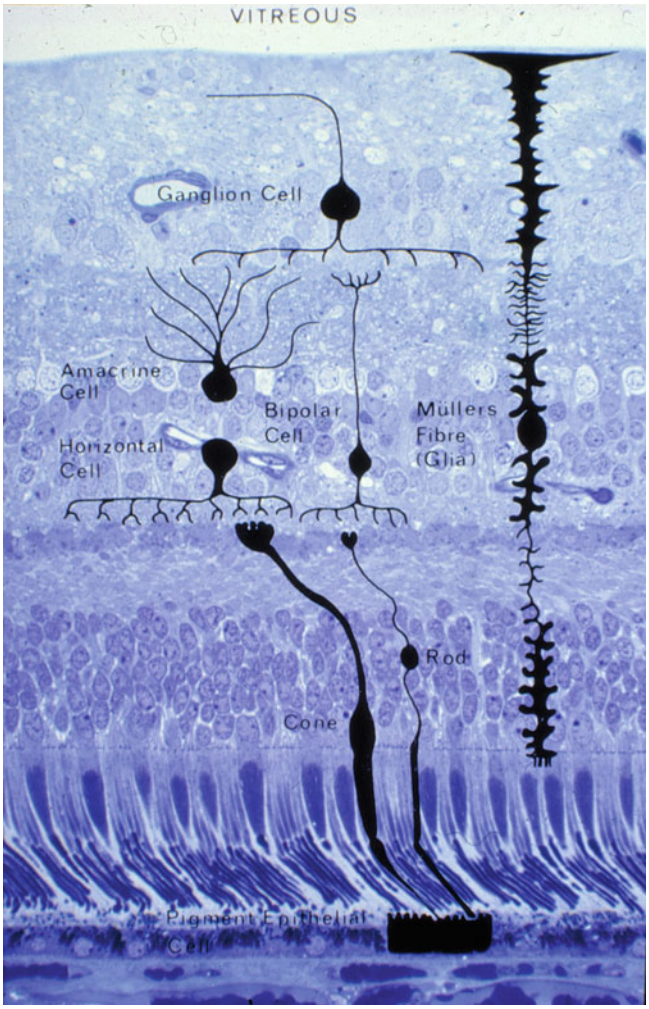

Fig. 1.6 The cell types are shown, and their positions in the retina are indicated (Courtesy of John Marshall)

Photoreceptor Layer

The photoreceptor transduces light into neuronal signals. The action of light closes gated cation channels leading to hyperpolarisation of the cell. Two types of photoreceptor exist, the rods predominantly in the periphery and absent from the fovea and the cones concentrated at the macula. They are made up of:

Outer Segments

Light is absorbed by the visual pigments which are contained in stacked discs. The discs are separate in the rods (1,000 in number) but are interconnected in the cones. These join to the inner segment by the cilium.

Inner Segments

These consist of an inner myoid which contains the Golgi apparatus and ribosomes for making cell structures and an outer ellipsoid which contains mitochondria for energy production. These connect to the nucleus by the outer connecting fibre. The inner connecting fibre connects to the synaptic region. The latter has synapses arranged as triads with connections to one bipolar cell and two horizontal cells. In cones, there may be up to 20 triads whereas the rods have only one.

Outer Limiting Layer

This consists of junctional complexes from the Muller cells and photoreceptors and is located at the inner connecting fibres.

Outer Plexiform Layer

The cell processes of the horizontal cells and bipolar cells synapse with the receptors.

Intermediary Neurones

Inner Nuclear Layer

This contains the cell bodies of the bipolar cells, the Muller cells, amacrine cells and horizontal cells.

Inner Plexiform Layer

The bipolar cells axons pass through, synapsing with the amacrine cells which help process the neuronal signals to the ganglion cells.

Ganglion Cells

Ganglion Cell Layer
The cell bodies of the ganglion cells are found here. These cells have gathered preprocessed information from the other retinal cells. The cells receive different visual information such as a sustained response to light, transient response or response to movement. At the macula, there is 1 ganglion cell to 1 receptor, but on average, in the whole retina, there is 1 for 130 receptors.

Nerve Fibre Layer
The nerve fibres of the ganglion cells on the inner surface of the retina pass tangentially towards the optic nerve.

Inner Limiting Membrane
Note: The internal limiting membrane (ILM) is a tough membrane laid down by the Muller cells with connections to the hyaloid membrane of the vitreous.

Retinal Blood Vessels

The central retinal artery supplies the neural retina with the exception of the photoreceptors which are supplied by the choriocapillaris. This is an end artery system with a single draining vessel, the central retinal vein. Both vessels have four main branches which divide at the optic disc to supply nasal and temporal quadrants. At the posterior pole, there is a capillary network at the level of the nerve fibre layer and the outer plexiform layer. In the periphery, there is one capillary network at the inner nuclear layer. The capillary endothelium forms the inner retinal blood–retinal barrier by having tight intercellular junctions.

Other Fundal Structures

Bruch's Membrane
A pentalaminar structure partly representing the basement membranes of the RPE and the choriocapillaris. It is of ectodermal and mesodermal origin. Accumulation of damage in Bruch's is seen in age-related macular degeneration.

Choroid
This is a vascular layer (large vessels are outer and the capillaries are inner) with a high relative blood flow and low oxygen utilisation (3 %). It supplies the RPE and photoreceptors. The highly anastomotic and fenestrated capillaries are arranged into lobules and are supplied by the posterior ciliary arteries and drained by the vortex veins.

1.1.3 The Physiology of the Vitreous

The physiology of the vitreous is not well understood. It is thought that molecules can move in the gel because of diffusion and convection and by the effects of saccades on the fluid component of the gel. Diffusion is most important for animals with smaller eyes, whereas convection is more important for larger eyes such as human eyes. Molecules with an anionic charge move more easily in the gel. Small soluble molecules like fluorescein move at a similar rate to aqueous; larger molecules like albumin may move 30–50 % less rapidly than aqueous (Xu et al. 2000). Convection is estimated to account for 30 % of movement of molecules in the vitreous because there is a pressure differential from the anterior ingress of aqueous to the posterior egress of fluid through the retina by the RPE pump. The saccadic movement of the eyes induces convection currents in the anterior vitreous which circulate around the vitreous base because of the effect of the indentation of the lens into the vitreous cavity (Repetto et al. 2010).

The measured viscosity of the vitreous depends on the technique used with estimates saying from 5–2,000 mPas (aqueous = 1 mPas). It is non-Newtonian, that is, a non-linear relationship and bimodal probably because there is a micro- and macro-viscosity component. The vitreous is relatively hypoxic (pO_2 of 30–40 mmHg) in comparison to air (150 mmHg) and arterial blood (100 mmHg) (Stefansson 2006). The relatively small proportion of ocular blood supply to the retina (2–3 %) has a profound effect on the vitreal PO_2 (Williamson and Harris 1994; Shui et al. 2009). There are oxygen gradients in the vitreous with higher PO_2 in the anterior vitreous than the posterior. Ascorbate concentrations are high in the vitreous; the ascorbate may react with oxygen to reduce the PO_2 (Shui et al. 2009).

The reason for low PO_2 in the vitreous is unknown, but it may be to protect the lens proteins from oxidation (Holekamp et al. 2005). Removal of the vitreous by vitrectomy causes nuclear sclerotic cataract except in ischemic eyes such as diabetic retinopathy and retinal vein occlusion (Holekamp et al. 2006). Inserting tamponade agents such as silicone oil into the vitreous cavity increases the concentration of ions, for example, K^+ and Ca^+ in the remaining aqueous layer in the cavity (Winter et al. 2000).

1.1.4 Anatomy and Physiology and the Vitreoretinal Surgeon

There are certain features of the anatomy and physiology that the surgeon should remember whilst operating.

At the ora serrata, the non-pigmented epithelium is continuous with the neurosensory retina, and, therefore, retinal detachments can extend anteriorly through the ora on rare

occasions. Ultimately, the ciliary body may be detached causing reduction in intraocular pressure (IOP) and even hypotony and choroidal effusion.

The posterior attachment of the vitreous base to the retina moves more posteriorly in the elderly (Bishop et al. 2004).

The nerve fibre layer orientation is especially important whilst working on the surface of the retina where damage to the nerve fibres might occur, for example, in macular hole surgery (Chap. 8).

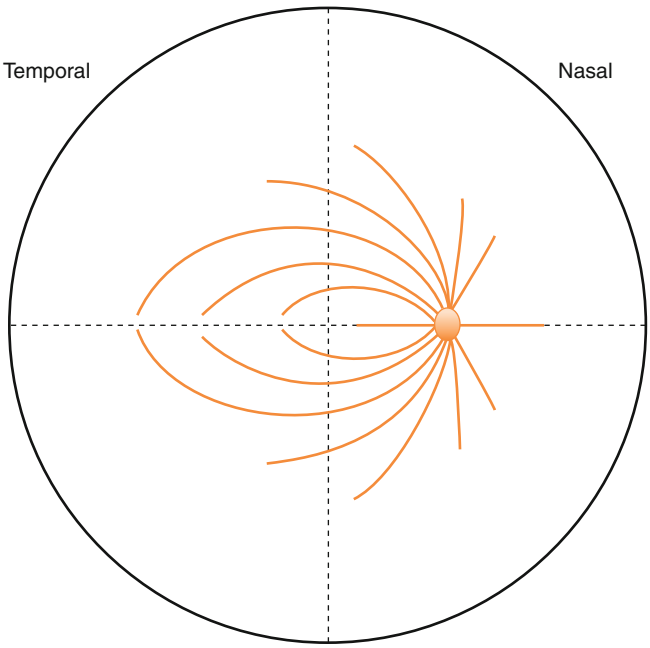

Fig. 1.7 Always consider in which direction the nerve fibres run on the surface of the retina when operating so as to minimise damage to the fibres. Try to cut or scrape along the direction of the nerve fibres rather than perpendicular to their direction

The fovea is the thinnest part of the retina and is therefore prone to dehiscence and hole formation during retinal elevation, for example, in macular surgery.

The force required to cause a retinal detachment has been put at approximately 200 dynes/cm^2 (approximately 0.27 mmHg, i.e. not very much) in primates. A number of mechanisms have been implicated in keeping the retina attached.

The retinal pigment epithelium applies forces to the retina: through ionic flow as calcium and magnesium move across the RPE, hydrostatic forces from the intraocular pressure and flow of fluid out of the eye. The RPE pump works against the relative resistance to fluid flow of the retina and has been estimated at 0.3 ml/h/mm^2.

Increased osmotic pressure exerted by the increased protein content in the choroidal circulation also encourages fluid flow across the retina.

In addition, there are intercellular components aiding adhesion of the retina to the RPE such as the interphotoreceptor matrix and interdigitation of rod outer segments with RPE microvilli.

Interestingly, evidence of vitreous collagen metabolism (C-propeptide levels of type II pro-collagen) (Itakura et al. 2005) is found in the vitreous cavity of vitrectomised eyes, although hyaluronan levels are reduced.

1.2 Clinical Examination and Investigation

1.2.1 Using the Database

Keeping an electronic patient record of the clinical details of the patient aids clinical audit and governance. A fully operational system has been provided which runs on Microsoft Access (you will need a copy of Access 2010

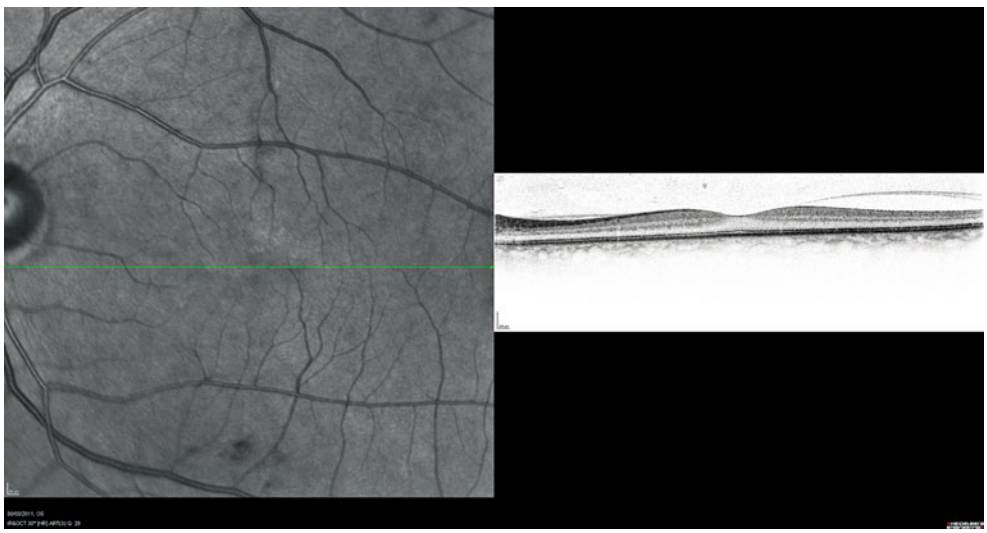

Fig. 1.8 The vitreous is more strongly attached to the fovea. The posterior hyaloid membrane can be seen detached from the temporal retina but still attached at the fovea and nasal to the fovea on optical coherence tomography (*OCT*)

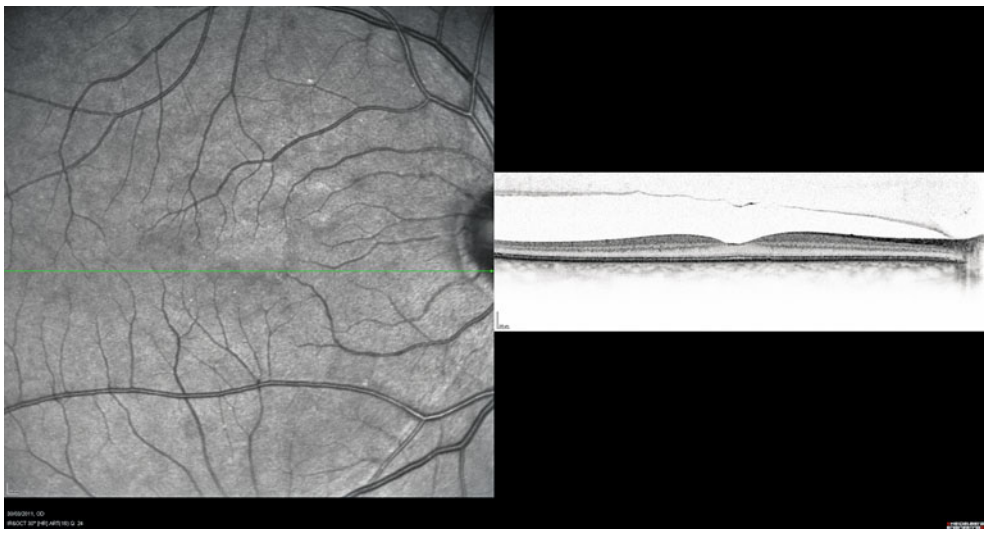

Fig. 1.9 The vitreous is more adherent to the optic nerve head. The posterior hyaloid membrane can be seen separated from the retina but attached to the optic nerve head

Table 1.1 Various lenses and their characteristics

Lens	Slit lamp or BIO	Field of view	Magnification	Depth perception	Uses	Periphery
20D	Bio	Good	Fair	Fair	Peripheral	Far periphery
28D	Bio	Very good	Poor	Poor	Small pupil or paediatric	Far periphery
90D	Slit lamp	Poor	Good	Fair	Small pupil	Posterior to the equator
Super-field	Slit lamp	Good	Good	Fair	General	Equator
60D	Slit lamp	Poor	Very good	Good	Macula	Not for the periphery
Goldmann three-mirror	Slit lamp	Poor	Very good	Good	General	Equator
Hruby lens	Slit lamp	Poor	Very good	Very good	Macula	Nil
Rodenstock	Slit lamp	Very good	Poor	Poor	Panretinal photo coagulation	Equator

to run the database) and follows the classification of disease used in this text. The structure of the database includes tables into which data is stored as a record. The main table is 'mailing list'; the other tables are linked to this (related) to store clinical data. There are forms to input data and reports for printing data out. Learn to create queries to analyse your data. A comprehensive manual has not been provided, but with trial and error, you should soon find your way around.

1.2.2 Examination of the Eye

1.2.2.1 Examination Technique

Visual Acuity

LogMar values are recommended for the ease of analysis of data for surgical audit and governance. This can be measured by Snellen chart or EDTRS chart but requires full refractive correction.

1.2.2.2 The Slit Lamp

The vitreoretinal surgeon must be able to use the slit lamp, Goldmann tonometry and various contact lenses or three-mirror contact lens and be able to visualise the vitreous by looking behind the posterior lens. The vitreous must be inspected for clarity, cellular infiltration and by asking the patient to move the eye to inspect the mobility of the vitreous. The slit lamp allows the use of specialised lenses for the examination of the vitreous and retina, for example, super-field, 90D or 60D lenses and noncontact lenses.

1.2.2.3 Binocular Indirect Ophthalmoscope

A principle extra skill required is the use of the binocular indirect ophthalmoscope with indentation of peripheral retina (Schepens 1947).

Method: Examine in a systematic manner. Always lay the patient flat on an examination couch preferably with no pillow.

Note: Commence examination standing at the patient's side whilst examining the 12 o'clock position of the retina, and move around the head of the patient to the other side of the patient systematically examining the whole of the peripheral retina returning to the 12 o'clock position.

Remember, the patient looks in the direction of the retina that the observer wishes to see; for example, if examining the superonasal retina, the patient looks superonasally. Initially examine the eye without indentation thereby orientating to the distribution of subretinal fluid (SRF) and to provide a clue to localisation of features such as retinal breaks according to Lincoff's rules (described in Chap. 5). Using indentation to examine the retina, move around the patient's head in the opposite direction finally returning to the original starting position.

1.2.2.4 Using the Indenter

The superior retina (and the temporal side) is often easier to examine because the upper lids are easier to indent through. Ask the patient to look down, place the indenter head on the lid above the tarsal plate and ask the patient to look up. As they do this, rotate the indenter superiorly and apply pressure in the globe aiming towards the centre of the eye.

Note: Get the feel for the required pressure to apply to the globe by pressing the indenter gently on your thumb just enough to depress the skin of the tip of your thumb. Try not to push back into the orbit which only succeeds in indenting the orbital septum and causing the patient discomfort.

Observe the indent on the retina whilst gliding the indenter back and forwards or from side to side. Watching the movement of the retina facilitates retinal tear detection. Aim to be able to examine the retina right up to the ora serrata; small anteriorly placed holes can be difficult to find and will cause failure of surgery if undetected. When examining the inferior retina, ask the patient to look up, place the indenter below the inferior tarsus and then ask the patient to look inferiorly. The horizontal positions are difficult to see because the canthal tendons and caruncle make indentation uncomfortable. Orientate the indenter vertically, place the indenter above or below these structures and move it sideways to move them out of the way for indentation.

Use a metal indenter, either the modified thimble variety or the pen-sized stick.

Fig. 1.10 Notice the sideways lean when examining with the indirect ophthalmoscope in order to avoid backache

1.2.2.5 Ultrasonography

Ultrasound is essential for the examination of the eye with medial opacities (Fig. 1.11).

Note: Learn to perform this technique. Ultrasound is a dynamic examination from which information can be rapidly obtained in the clinical setting.

Ultrasound has a frequency, number of cycles/s of 20 hertz (Hz) which is inaudible to human ears. The higher the frequency of the ultrasound (the shorter the wavelength), the higher is the resolution but at the cost of less penetration into tissues.

Appropriate frequencies for ophthalmology vary from 7.5 to 10 MHz for the posterior segment and with 20–50 MHz for the anterior segment.

Sound travels faster through solids than liquids, for example, through both aqueous and vitreous at 1,500 metres/second (m/s) and through the cornea and lens at 1,650 m/s. Therefore, clear images are readily available from the eye and orbit.

Sound is reflected when it encounters an interface of different tissue densities resulting in an echo whose strength relates to the difference in the densities. The signal is highest when the interface is perpendicular to the ultrasound beam.

In B-scan ultrasonography, an oscillating sound beam is emitted, and the signal is reconstructed to produce a 2D image of the tissue.

Some tissues will absorb the sound waves (e.g. a dense cataract) reducing the signal from more posteriorly placed tissues.

Normally, the vitreous is echolucent.

When performing the scan, the operator should be seated and facing the patient and the machinery. For a short scan, the patient may be seated, but if a prolonged scan is proposed, the supine positioning of the patient is recommended to avoid fatigue of the observer's arm. The examiner should hold the probe in the dominant hand and place the lead around the shoulders to support the weight of the ultrasound cable during the examination. Perform the scan with contact jelly on the closed eyelids of the patient. Increase the gain to allow visualisation of the vitreous but without producing artefacts. Detect the lens (two bracket-shaped echoes anteriorly) and

Fig. 1.11 B-scan ultrasound is essential for the running of a vitreoretinal clinic and should be present in every clinic and operated primarily by the vitreoretinal surgeon himself for interpretation of the dynamic signs in the eye

Fig. 1.12 Moving the eye from side to side shows mobility of the vitreous in this patient with subhyaloid haemorrhage

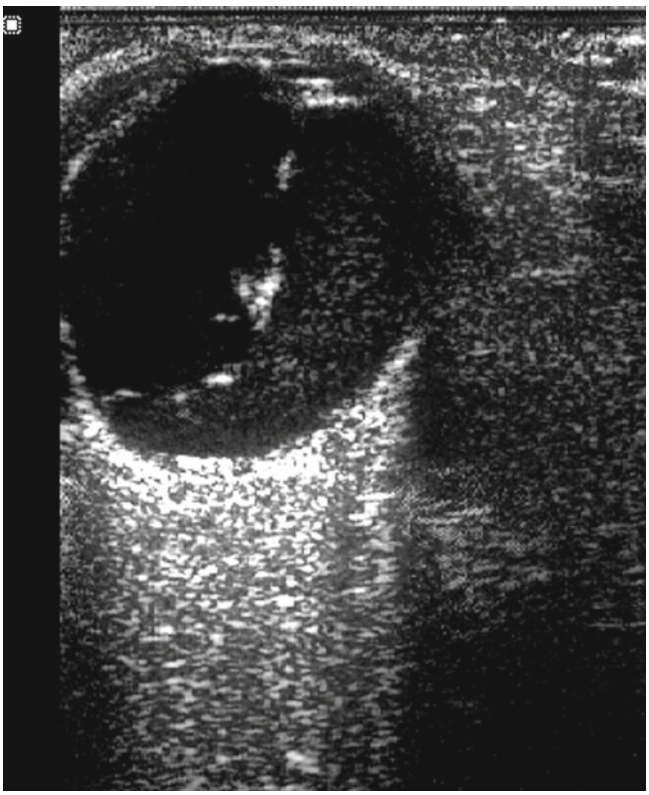

Fig. 1.13 Ultrasound left

the optic nerve (an echolucent band extending from the posterior pole) to check your alignment and to orientate yourself in the eye. Perform horizontal scans asking the patient to look right and left to detect the dynamic properties of the tissues and then vertical scans with eye movements up and down. To inspect a particular region of the eye, ask the patient to look in the direction of the region of interest, for example, up and left for the superotemporal area of the left eye. With this dynamic technique, information can quickly be gathered regarding the anatomy and pathology of the vitreous, retina and choroid. Furthermore, colour Doppler ultrasound can be used to detect blood vessels in the retina in suspected retinal detachment in complex cases such as trauma (Wong et al. 1991).

Abnormalities are seen in:

- Asteroid hyalosis
- Multiple small, highly reflective vitreous opacities
- Vitreous haemorrhage (Figs. 1.12, 1.13)

Diffuse fine echoes or clumps of organised clot are seen in the vitreous cavity often with diffuse haemorrhage behind the posterior hyaloid (subhyaloid haemorrhage). Clot on the posterior cortex especially inferiorly can be

Fig. 1.14 The sinuous shape of a recent onset retinal detachment. Notice how the retina attaches into the optic nerve head and the vitreous can be seen anteriorly

Fig. 1.15 Retinal detachments have a sinuous mobility on ultrasound and an attachment at the optic disc

mistaken for retina. If no attachment to the disc is seen, this will usually rule out retinal detachment; however, sometimes, there are disc attachments of the vitreous to disc new vessels.

Fig. 1.16 Colour Doppler imaging can be used to detect blood vessels to confirm that an echo is representative of the retina

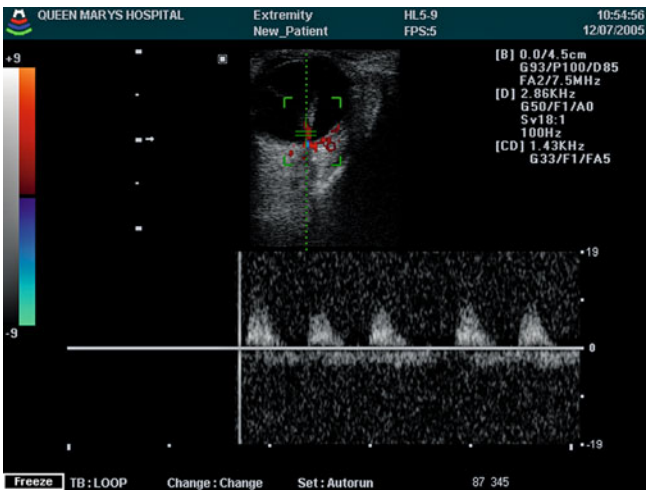

Fig. 1.17 Pulse Doppler imaging can be used to detect blood vessels to confirm that an echo is representative of the retina, notice the retinal artery above the line and the retinal vein below

Posterior Vitreous Detachment (PVD)

The posterior hyaloid membrane is seen as a low continuous and sinuous echo which whips around the eye with eye movements.

Retinal Tear

The flap of a retinal tear may be seen in a patient with vitreous haemorrhage and posterior vitreous detachment. Most tears that produce haemorrhage are large; therefore, there is a chance of seeing the break on ultrasound. However, it is not safe to assume that there is no break if none is detected on ultrasound.

Retinal Detachment

A highly reflective, undulating membrane from the ora serrata anteriorly and the optic nerve posteriorly indicates retinal detachment. Initially mobile, this stiffens and shortens with the development of proliferative vitreoretinopathy (PVR).

Subretinal Haemorrhage

Often seen in choroidal neovascularisation (CNV) is vitreous haemorrhage with a craggy mass of subretinal blood in the macula.

Retinoschisis

This is smooth, dome-shaped, less mobile and thinner than rhegmatogenous retinal detachment (RRD).

Choroidal Elevation

Choroidal effusions are smooth, dome-shaped, immobile and thick with a high signal. If haemorrhage is present, the suprachoroidal fluid is diffusely echogenic. Tumours have a vascular circulation on colour Doppler.

Trauma

The above features can be discriminated to determine the degree of injury in a blood-filled eye. In addition, features such as intraocular foreign bodies can be detected as a high reflection with shadow. Even eyes with scleral rupture can be examined. Use plenty of contact jelly so that the probe can be placed on the eye with no pressure applied to the globe.

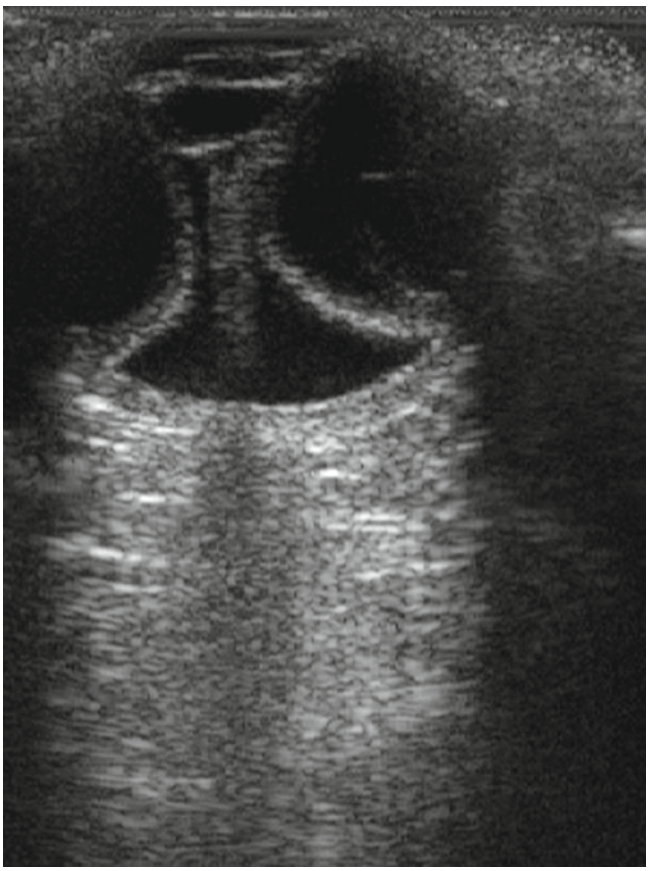

Fig. 1.18 On ultrasound, choroidal effusions have a smooth dome-shaped outline. The choroidal effusions can touch centrally, 'kissing choroidals'; surgically these can be separated (they are sometimes mildly adherent), but initially you may need to infuse through the anterior chamber because there is no space to insert the pars plana infusion until the choroidals are drained

Fig. 1.19 Ultrasound reveals a choroidal haemorrhage which can be measured

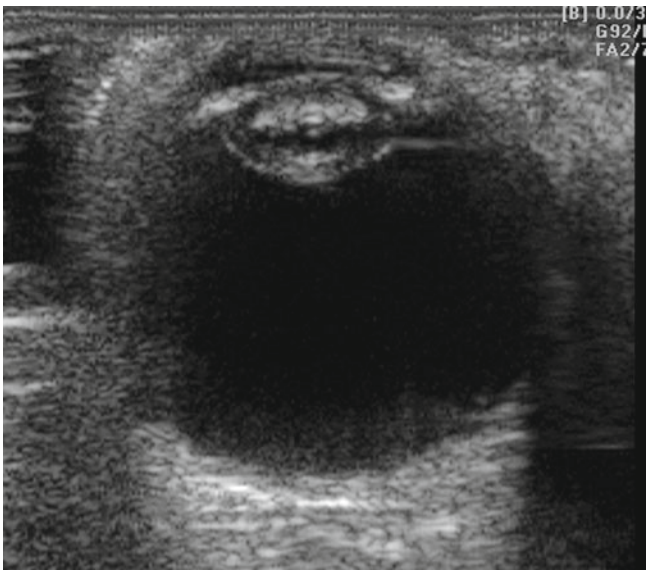

Fig. 1.20 The cataract in this patient is clearly seen and can attenuate the signal from more posteriorly

1.2.2.6 Optical Coherence Tomography

Optical coherence tomography (OCT), first developed for ophthalmic imaging in the 1990s (Huang et al. 1991), is invaluable in the retinal clinic. OCT scanning provides two-dimensional cross sections of the retina from which three-dimensional reconstructions can be created (Hee et al. 1995).

The first-generation (TD-)OCTs were only capable of resolutions between 10 and 20 μm because they relied on the mechanical movement of a mirror to measure the time taken for light to be reflected and were therefore relatively slow to perform. These have been superseded by spectral domain OCTs (SD-OCTs) that are able to simultaneously measure multiple wavelengths of reflected light and have reported

Fig. 1.21 OCT machinery has now become commonplace in vitreoretinal clinics and is extremely useful for discriminating different types of macular pathology

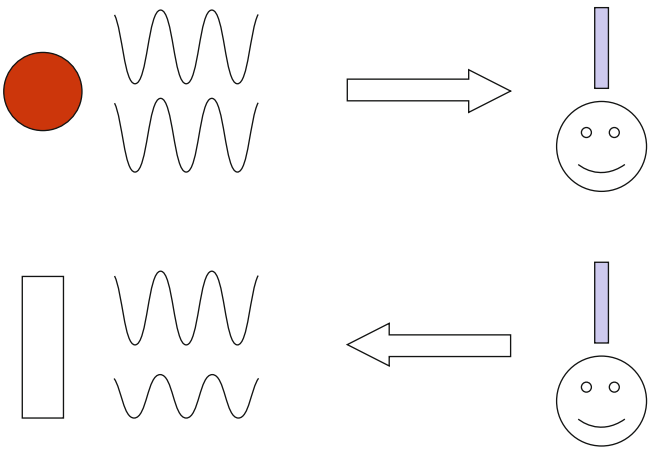

Fig. 1.22 OCT uses a reference laser compared to a laser which has been directed at an object of interest. The incoherence of the two lasers is then used to interpret the signal from the object of interest to provide *z*-axis information and intensity information

resolutions up to 5–6 μm. With higher-resolution scanning, a cross-sectional B-scan can reveal most layers within the neurosensory retina (Chan et al. 2006). A few histological studies have correlated the OCT appearance with histological sections of human and animal retinas (Hoang et al. 2002; Gloesmann et al. 2003). Further studies have correlated the segmentation (bands) on an OCT with retinal layers by sequentially ablation of these layers surgically (Chauhan and

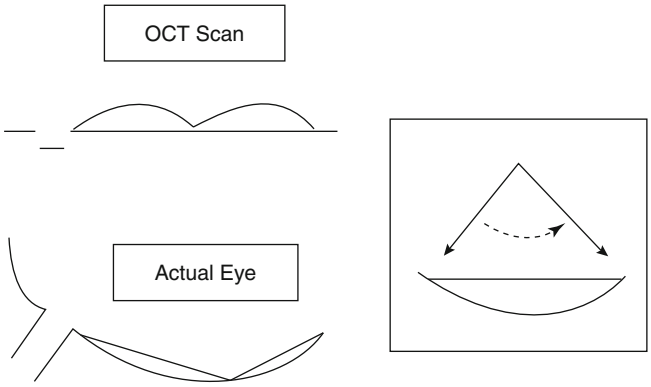

Fig. 1.23 With most OCT scanners, the posterior pole of the eye has been falsely flattened; the images should be interpreted with this in mind

Marshall 1999; Ghazi et al. 2006). The outer red line is frequently assumed to represent the RPE alone but in actuality corresponds with the highly reflective chorioretinal complex as a whole.

Time-Domain OCT

Conceptually, OCT operates on the same physical principles as an ultrasound scan except it uses light as the carrier signal. As such, the spatial resolution of an OCT is much higher than conventional 10–20-MHz ultrasound as a result of the naturally shorter wavelength of light. The source of light in an OCT is produced by a superluminescent diode, femtosecond laser or more recently using white light (Sacchet et al. 2008).

OCT works by splitting a beam of light into two arms – a reference arm and a sampling arm. First-generation OCTs are time-domain OCT (TD-OCT), so named because the length of the reference arm is varied with time, in order to correlate with the back-reflected sample arm. This is achieved with the use of an adjustable mirror of known distance within the device. The sample arm is focused onto the retina with the use of an in-built 78D lens. The sample beam is reflected off the structures in the eye and is recombined with the reference beam by using a Michelson interferometer within the unit. A single cycle of this process yields 1 A-scan. This single scan comprises data on the distance the sample arm has travelled and the back-reflectance and backscatter of the beam. Tissue layers at varying depths and optical characteristics produce differing reflective intensities. As in an ultrasound scan, in order to produce a B-scan image, multiple A-scans are obtained in rapid succession across the area of interest. Software combines this information to produce a two-dimensional image either in greyscale or with arbitrary false colouring. The result is a cross-sectional scan, a reconstructed three-dimensional topographical image,

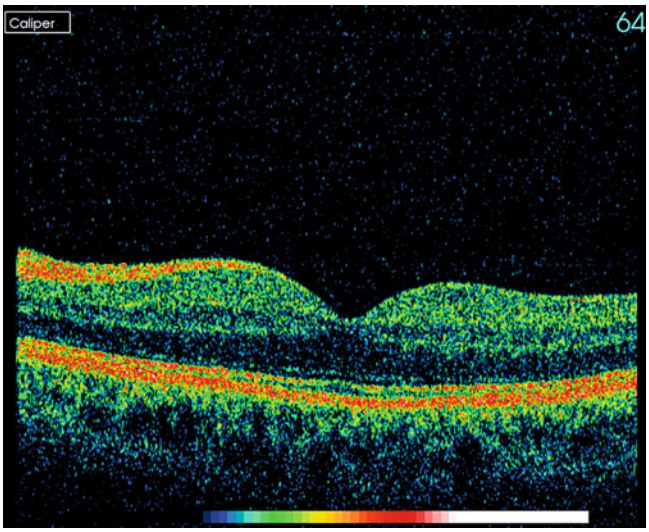

Fig. 1.24 OCT provides a cross-sectional scan of the macula which provides essential information to diagnose disorders and plan surgery

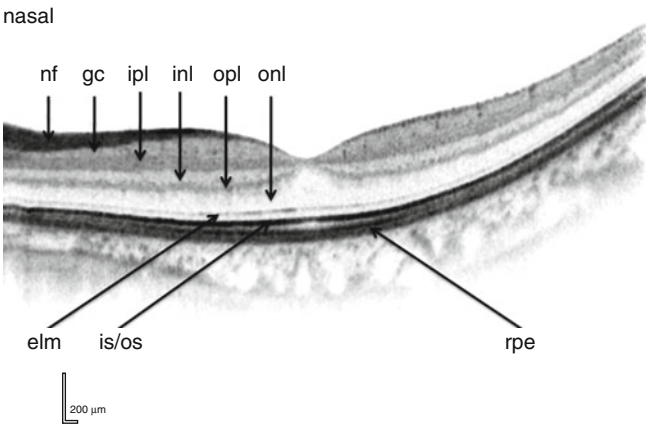

Fig. 1.25 With high-resolution OCT B-scan image of the normal human macula, the individual layers of the retina can be seen. Note resolution is usually better with greyscale rendering. *NF* nerve fibre layer; *GC* ganglion cell layer, *IPL* inner plexiform layer, *INL* inner nuclear layer, *OPL* outer plexiform layer; *ONL* outer nuclear layer, *ELM* external limiting membrane, *IS/OS* photoreceptor inner Segment and outer segment junction, *RPE* retinal pigment epithelium and inner choroidal layers

quantitative thickness measurements or more recently z-plane or coronal scans (Sacchet et al. 2008).

Colour Coding

Reflection	Nil	Black
Low	Green	
Mod	Red	
High	White	

Frequency-Domain OCT

Unlike TD-OCT, frequency-domain OCT (FD-OCT) generates the axial scan by Fourier transformation of the acquired spectral interference fringes generated by the interaction of the reference and sample arms. Therefore, the reference arm in an FD-OCT does not have to move, allowing dramatically quicker scan acquisition speeds than is possible by TD-OCT.

Spectral-domain OCT (SD-OCT), also known as Fourier-domain OCT, is based upon the underlying principle of FD-OCT, but SD-OCT is able to extract more information in a single scan as it distributes several optical frequencies onto a detector stripe (Bourquin et al. 2001).

Time-encoded FD-OCT, also known as swept-source OCT (SS-OCT), is again based on FD-OCT. However, unlike Fourier-domain OCT which emits multiple optical frequencies all at once, the swept-source OCT emits multiple frequencies in single successive steps. SS-OCT is at present not commercially available but has shown promise in recent studies which have demonstrated significantly improved resolution and image penetration for imaging structures and pathology deep to the retina because it operates in the 1,050-nm wavelength range (Yasuno et al. 2009; Srinivasan et al. 2008).

Full-Field OCT

The latest-generation OCT is the full-field OCT (FF-OCT), another version of the TD-OCT, which uses a broadband (white) light source instead of a laser or superluminescent diode (Sacchet et al. 2008). Also known as T-scan (transverse) OCT or en face OCT, it acquires tomographic data by acquiring multiple coronal scans instead of the usual axial scans (A-scans) of previously described TD-OCT (Rosen et al. 2009). SS-OCT is also capable of this scanning scheme (Potsaid et al. 2008). The advantage of this method is that it is not only possible to generate B-scans but also C-scans (coronal) alongside a simultaneous, conventional fundus image (coronal plane).

Scan Resolution

Obtaining a scan requires sequential scanning in the form of multiple A-scans for TD-OCT and SD-OCT and C-scans for FF-OCT. The volume of information obtained can be measured in volumetric pixels (voxels) (Potsaid et al. 2008). Increasing the number of voxels captured can be achieved by either increasing the scanning frequency rate, using multiple detector arrays or both (Bourquin et al. 2001; Potsaid et al. 2008). Commercially available SD-OCT scanners became available in early 2006, and most have imaging speeds of 25,000 axial scans/s with an axial resolution of between 5 and 7 µ. Technological optimisation of these variables has produced OCT scanners which achieve up to 250,000 axial scans/s whilst maintaining axial resolution at 8–9 µ, thus yielding more than 100 megavoxels (Potsaid et al. 2008). Clinically, this translates into a high-resolution macular scan in 1.3 s or even the potential to measure blood flow velocities

Scan of normal features

Device	Manufacturer	Technology	Signal wavelength	Scan speed (A-scans)	Axial resolution (μm)	Transverse resolution (μm)	Scanning field	Macular depth range (mm)	Additional features
STRATUS OCT™ Optical Coherence Tomography	Carl Zeiss Meditec, Inc.	TD-OCT	820-nm (NIR) SLD	400	≤10	20	26° × 20.5°	2	
RTVue-100	Optovue	SD-OCT	840 nm (NIR)	26,000	5	15	32° × 23°	2	
Cirrus™ HD-OCT Optical Coherence Tomography Instrument	Carl Zeiss Meditec, Inc.	SD-OCT	840-nm SLD	27,000	5	15	36° × 30°	2	Line-scanning ophthalmoscope
SPECTRALIS® OCT	Heidelberg Engineering, Inc.	SD-OCT	820-nm laser Diode and 870-nm SLD	40,000	3.9	14	55°	1.8	Active eye tracking
SPECTRALIS® OCT PLUS	Heidelberg Engineering, Inc.	SD-OCT	820-nm laser diode and 870-nm SLD	40,000	3.9	14	55°–150°	1.8	Active eye tracking Peripheral and wide-field OCT
3D OCT-1000 Mark II	Topcon Medical Systems	SD-OCT	840-nm SLD	18,000	5–6	≤20	8.2 × 3 mm (45°)	2.3	Colour non-mydriatic retinal camera
SOCT Copernicus HR	Optopol Technology	SD-OCT	850-nm SLD	52,000	3	12–18	10 mm	2	
Spectral OCT/SLO	OPKO Instruments/OTI	SD-OCT	830-nm SLD	27,000	5–6	20	29°	2	Registration with SLO, microperimetry
Bioptigen SD-OCT	Bioptigen	SD-OCT	820 nm (NIR)	17,000	4.5	15	50°	2	Handheld OCT (60°)

in vessels as narrow as 13.64 μm (Wang and An 2009; Tao et al. 2009). Higher scanning speeds are less likely to suffer from motion artefact (Srinivasan et al. 2006). Signal strength is the measure of the amount of reflected light received by the scanner. It is graded to serve as a proxy measure of scan quality. A signal strength of at least seven should be aimed for in order to obtain consistently accurate results (Wu et al. 2007, 2009). High scan rates can reduce signal strengths to below this (Potsaid et al. 2008).

Images and Measurements

Software-controlled scanning protocols translate voxel datasets into clinically representative images and are numerous. Post-scan software processing also determines surface segmentations like the internal limiting membrane (ILM) and retinal pigment epithelium (RPE) amongst others and assigns a false colour to each layer depending on the signal reflectance. However, greyscale and proportion-corrected OCT images reveal a finer gradation of signal reflectance and can be used to demonstrate additional information not present in false-colour images (Ishikawa et al. 2000). Software outlining of the ILM is necessary for calculation of retinal thickness; however, it has been shown to be inaccurate in up to 19 % of scans (Haeker et al. 2006). Hence, new algorithms are being constantly developed to overcome these shortfalls (Garvin et al. 2009; Sadda et al. 2007; Haeker et al. 2006). Results depended more on the algorithm used than the hardware, emphasising the need for robust software (Hood et al. 2009). The clinician should check the image used in analysis because artefacts exist (43.2 % in one study, with 30 % requiring manual remeasurement due to spurious central point thickness (CPT)) (Domalpally et al. 2009).

Performing the Scan

The rapid, noncontact, non-invasive nature of OCT scanning lends itself to the busy vitreoretinal clinic.

- Obtaining an OCT image requires mydriasis to ensure an artefact-free scan. Non-mydriatic scanning is possible but may result in vignetting of the macular scan as the edges of the sample beam are clipped by the pupillary margin. If it is not possible to dilate the patient, then scanning in a dark environment would reduce this phenomenon as the vast majority of OCT scanners use near-infrared light which does not induce papillary constriction.
- The macula is visualised on the monitor and the area of interest aligned with the aid of fixation targets. It is useful to ensure the patient blinks several times prior to acquiring the scan to ensure an even tear film. Even the presence of contact lenses can affect retinal nerve fibre layer thickness measurements (Youm et al. 2009). Dense media opacities will degrade image quality though OCT is able to quite effectively penetrate most cataracts, asteroid hyalosis and vitritis. Mathematical models have been developed to improve the quality of these degraded images (Tappeiner et al. 2008); however, the experienced examiner is usually still able to discern sufficient detail in most cases.

Macular Scan Patterns

- Radial scans, 'spokes of a wheel' centred on the fovea
- Raster, parallel lines creating a 'square'
- Single high-resolution line scans

On the 'fast macular thickness map' protocol with TD-OCT scanning, 6 radial sampling scans of the macula are acquired, and a macular topographical colour-coded map of the macula is produced. The software interpolates adjacent thickness values in the interspersing macular areas which lie between the 6 radial scans. Clinicians should therefore be aware of small lesions suspected to lie within these areas as they may fail to be picked up with this protocol. This is not an issue with the newer SD-OCT which acquires a raster series of high-resolution images (Srinivasan et al. 2006).

Central Retinal Thickness

Central retinal thickness, CRT, is the simplest measure to use and has been quoted in numerous studies. CRT was compared between 6 commercially available OCT scanners in a study involving healthy eyes, and a variation of between 0.45 and 3.33 % was found. The discrepancies were explained by the slightly different segmentation algorithms employed by each device (Wolf-Schnurrbusch et al. 2009). In effect, this means that the line which the software uses to determine the outer retinal boundary differs, and so different OCT systems should not be used interchangeably (Wolf-Schnurrbusch et al. 2009; Sayanagi et al. 2009).

Inner Segment and Outer Segment Junction and External Limiting Membrane

The predominant contribution to this 'outer red line' is by the Bruch's membrane and inner choroid with a smaller contribution by the RPE (Ghazi et al. 2006). Of particular interest is the band correlating to the junction of the inner and outer segment (IS/OS) of the photoreceptors. This is better visualised as a red line just inner to the outer red line (ORL) on the higher-resolution SD-OCT. The IS/OS band is a high-reflectance signal at this junction resulting from the abrupt change in the refractive index stemming from the highly organised stacks of membranous discs in the photoreceptor outer segments (Chan et al. 2006). Optical coherence tomographic changes in this area have been studied in a number of conditions, and visual acuity has been significantly correlated with OCT detection of the IS/OS junction in retinitis pigmentosa (Aizawa et al. 2009), macula-off retinal detachments (Wakabayashi et al. 2009), full-thickness macular holes (Sano et al. 2009; Baba et al. 2008; Inoue et al. 2009), central serous chorioretinopathy (Piccolino et al. 2005), age-related macular degeneration (Sayanagi et al. 2009) and

macular oedema associated with branch retinal vein occlusions (Ota et al. 2008; Murakami et al. 2007).

The external limiting membrane (ELM) appears to show prognostic promise (Wakabayashi et al. 2009). In a series of consecutive retinal detachments (RD), IS/OS disruption was observed in macula-off eyes. As predicted, postoperative VA was significantly correlated with IS/OS integrity. None of the eyes with preoperative disruption of ELM and IS/OS regained postoperative IS/OS integrity. In contrast, 7 of 11 eyes which had intact ELM on OCT preoperatively regained the IS/OS junction during follow-up (Wakabayashi et al. 2009).

The inner retina has moderate reflectance, receptors low reflectance and the RPE shows high scatter from melanin. The laser is thereafter blocked, and no information from the choroid is usually obtained. Measurements of the tissues in

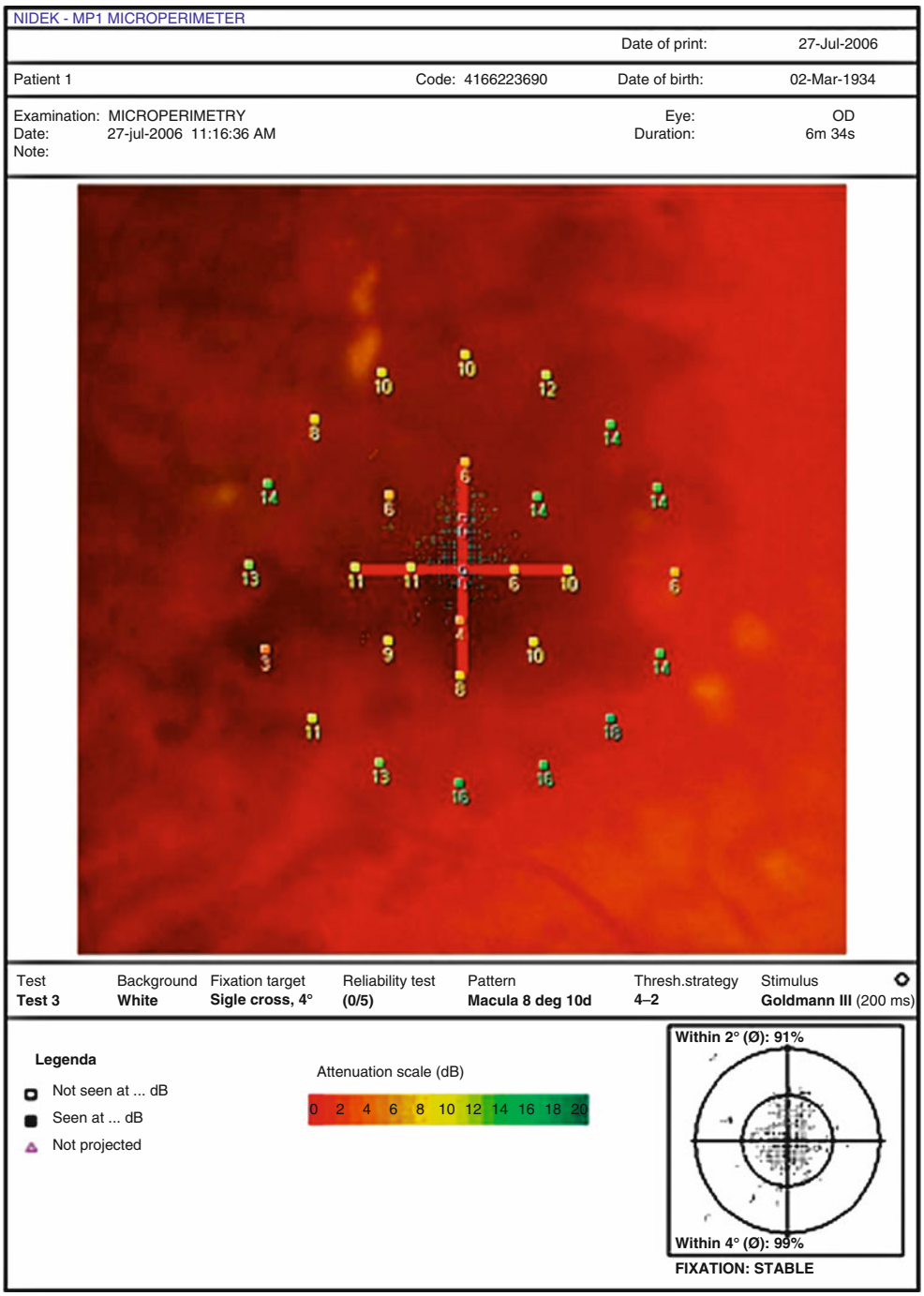

Fig. 1.26 Microperimetry is a useful tool to determine the fixation of the eye and detect localised loss of vision in the macula

the z axis are possible to quantify retinal thickness and volume.

OCT is useful for a variety of macular disorders such as macular holes, cystoid macular oedema, epiretinal membranes and choroidal neovascular membranes and in retinoschisis in myopes and optic disc anomalies. In macular holes, OCT is used for detection, differentiation from pseudo- and lamellar holes and for staging. OCT can be used for detection and monitoring of the cystoid macular oedema (CMO) in diabetes, retinal vein occlusion and in uveitis and for identifying vitreomacular traction.

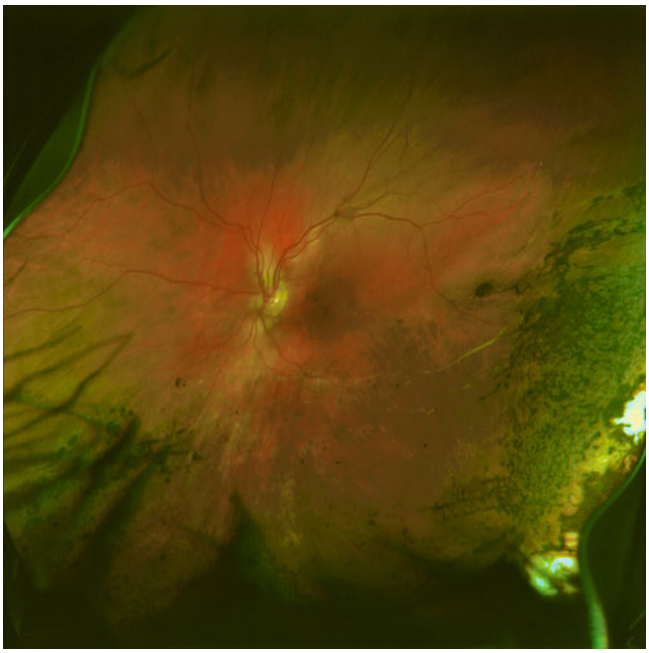

Fig. 1.27 In primary care, wide-angle laser imaging systems are sometimes used to view the retina. There are pigmentary changes in the periphery where a retinal detachment has reattached

1.2.3 Subjective Tests

The vitreoretinal patient often complains of symptoms which are related to the dysfunction of the macula such as distortion and change in image size. At present, the methods available to assess these are limited. Amsler charts can be used at the most basic level to determine distortion, alternatively use the ipad app Morphision. The Watzke Allen test (see Chap. 8) is used to discriminate macular holes from pseudoholes or partial-thickness holes in the fovea.

1.2.4 The Preoperative Assessment

Every patient should be thoroughly examined before surgery, at most 2 weeks before surgery. The situation with vitreoretinal conditions can change rapidly, for example, the development of proliferative vitreoretinopathy in rhegmatogenous retinal detachment. Make sure you know the status of the vitreous preoperatively, that is, is it attached or detached (perform ultrasound when there are medial opacities). Biometry for lens implantation is useful in case a cataract extraction is required unexpectedly during surgery. Use information sheets make sure the patient is realistic about outcomes and the risks for reoperation. Help them with the choice of anaesthesia. Mark the forehead on the side of the eye to be operated upon on the day of surgery with an indelible marker pen.

Table 1.2 Advantages and disadvantages of anaesthesia

Types of anaesthesia		Advantages	Disadvantages
General		Complete control of the eye during surgery No peroperative stress for the patient Allows peroperative examination of the fellow eye Patient does not hear surgeons' conversation during training	Risk to general health Longer recovery for the patient postoperatively May require inpatient admission
Local anaesthesia	All	Day-case surgery Minimal risk to general health	Patient stress levels Patient aware of conversations during training
	Peribulbar	Minimal soft tissue injury More effective anaesthesia and akinesia	Risk of globe perforation Difficult to top up during surgery Patient may see instrument close to the retina if the optic nerve is not blocked
	Sub-Tenon's cannula	Minimal risk of globe rupture Can be applied after draping Can be topped up Projects anteriorly deep-set globes for easier surgical access	Less effective anaesthesia and akinesia Poor application leads to conjunctival chemosis

1.3 Summary

A working knowledge of the anatomy of the retina is of great importance to the surgeon. Learn to examine the eye to a high standard, and obtain the basic investigational skills of ocular ultrasonography and optical coherence tomography.

References

Aizawa S, Mitamura Y, Baba T, Hagiwara A, Ogata K, Yamamoto S (2009) Correlation between visual function and photoreceptor inner/outer segment junction in patients with retinitis pigmentosa. Eye (Lond) 23(2):304–308. doi:10.1038/sj.eye.6703076, pii: 6703076

Baba T, Yamamoto S, Arai M, Arai E, Sugawara T, Mitamura Y, Mizunoya S (2008) Correlation of visual recovery and presence of photoreceptor inner/outer segment junction in optical coherence images after successful macular hole repair. Retina 28(3):453–458. doi:10.1097/IAE.0b013e3181571398, pii: 00006982-200803000-00009

Bishop PN, Holmes DF, Kadler KE, McLeod D, Bos KJ (2004) Age-related changes on the surface of vitreous collagen fibrils. Invest Ophthalmol Vis Sci 45(4):1041–1046

Bourquin S, Seitz P, Salathe RP (2001) Optical coherence topography based on a two-dimensional smart detector array. Opt Lett 26(8):512–514, pii: 63959

Chan A, Duker JS, Ishikawa H, Ko TH, Schuman JS, Fujimoto JG (2006) Quantification of photoreceptor layer thickness in normal eyes using optical coherence tomography. Retina 26(6):655–660. doi:10.1097/01.iae.0000236468.33325.74, pii: 00006982-200607000-00011

Chauhan DS, Marshall J (1999) The interpretation of optical coherence tomography images of the retina. Invest Ophthalmol Vis Sci 40(10):2332–2342

Domalpally A, Danis RP, Zhang B, Myers D, Kruse CN (2009) Quality issues in interpretation of optical coherence tomograms in macular diseases. Retina 29(6):775–781. doi:10.1097/IAE.0b013e3181a0848b

Garvin M, Abramoff M, Wu X, Russell S, Burns T, Sonka M (2009) Automated 3-D intraretinal layer segmentation of macular spectral-domain optical coherence tomography images. IEEE Trans Med Imaging. doi:10.1109/TMI.2009.2016958

Ghazi NG, Dibernardo C, Ying HS, Mori K, Gehlbach PL (2006) Optical coherence tomography of enucleated human eye specimens with histological correlation: origin of the outer "red line". Am J Ophthalmol 141(4):719–726. doi:10.1016/j.ajo.2005.10.019, pii: S0002-9394(05)01106-2

Gloesmann M, Hermann B, Schubert C, Sattmann H, Ahnelt PK, Drexler W (2003) Histologic correlation of pig retina radial stratification with ultrahigh-resolution optical coherence tomography. Invest Ophthalmol Vis Sci 44(4):1696–1703

Haeker M, Abramoff M, Kardon R, Sonka M (2006) Segmentation of the surfaces of the retinal layer from OCT images. Med Image Comput Comput Assist Interv Int Conf Med Image Comput Comput Assist Interv 9(Pt 1):800–807

Hee MR, Izatt JA, Swanson EA, Huang D, Schuman JS, Lin CP, Puliafito CA, Fujimoto JG (1995) Optical coherence tomography of the human retina. Arch Ophthalmol 113(3):325–332

Hoang QV, Linsenmeier RA, Chung CK, Curcio CA (2002) Photoreceptor inner segments in monkey and human retina: mitochondrial density, optics, and regional variation. Vis Neurosci 19(4):395–407

Holekamp NM, Shui YB, Beebe DC (2005) Vitrectomy surgery increases oxygen exposure to the lens: a possible mechanism for nuclear cataract formation. Am J Ophthalmol 139(2):302–310. doi:10.1016/j.ajo.2004.09.046, pii: S0002-9394(04)01147-X

Holekamp NM, Shui YB, Beebe D (2006) Lower intraocular oxygen tension in diabetic patients: possible contribution to decreased incidence of nuclear sclerotic cataract. Am J Ophthalmol 141(6):1027–1032

Hood DC, Raza AS, Kay KY, Sandler SF, Xin D, Ritch R, Liebmann JM (2009) A comparison of retinal nerve fiber layer (RNFL) thickness obtained with frequency and time domain optical coherence tomography (OCT). Opt Express 17(5):3997–4003, pii: 176995

Huang D, Swanson EA, Lin CP, Schuman JS, Stinson WG, Chang W, Hee MR, Flotte T, Gregory K, Puliafito CA et al (1991) Optical coherence tomography. Science 254(5035):1178–1181

Inoue M, Watanabe Y, Arakawa A, Sato S, Kobayashi S, Kadonosono K (2009) Spectral-domain optical coherence tomography images of inner/outer segment junctions and macular hole surgery outcomes. Graefes Arch Clin Exp Ophthalmol 247(3):325–330. doi:10.1007/s00417-008-0999-9

Ishikawa H, Gurses-Ozden R, Hoh ST, Dou HL, Liebmann JM, Ritch R (2000) Grayscale and proportion-corrected optical coherence tomography images. Ophthalmic Surg Lasers 31(3):223–228

Itakura H, Kishi S, Kotajima N, Murakami M (2005) Vitreous collagen metabolism before and after vitrectomy. Graefes Arch Clin Exp Ophthalmol 243(10):994–998. doi:10.1007/s00417-005-1150-9

Murakami T, Tsujikawa A, Ohta M, Miyamoto K, Kita M, Watanabe D, Takagi H, Yoshimura N (2007) Photoreceptor status after resolved macular edema in branch retinal vein occlusion treated with tissue plasminogen activator. Am J Ophthalmol 143(1):171–173. doi:10.1016/j.ajo.2006.08.030, pii: S0002-9394(06)01014-2

Ota M, Tsujikawa A, Murakami T, Yamaike N, Sakamoto A, Kotera Y, Miyamoto K, Kita M, Yoshimura N (2008) Foveal photoreceptor layer in eyes with persistent cystoid macular edema associated with branch retinal vein occlusion. Am J Ophthalmol 145(2):273–280. doi:10.1016/j.ajo.2007.09.019, pii: S0002-9394(07)00829-X

Piccolino FC, de la Longrais RR, Ravera G, Eandi CM, Ventre L, Abdollahi A, Manea M (2005) The foveal photoreceptor layer and visual acuity loss in central serous chorioretinopathy. Am J Ophthalmol 139(1):87–99. doi:10.1016/j.ajo.2004.08.037, pii: S0002-9394(04)01006-2

Potsaid B, Gorczynska I, Srinivasan VJ, Chen Y, Jiang J, Cable A, Fujimoto JG (2008) Ultrahigh speed spectral/Fourier domain OCT ophthalmic imaging at 70,000 to 312,500 axial scans per second. Opt Express 16(19):15149–15169, pii: 171960

Repetto R, Siggers JH, Stocchino A (2010) Mathematical model of flow in the vitreous humor induced by saccadic eye rotations: effect of geometry. Biomech Model Mechanobiol 9(1):65–76. doi:10.1007/s10237-009-0159-0

Rosen RB, Hathaway M, Rogers J, Pedro J, Garcia P, Laissue P, Dobre GM, Podoleanu AG (2009) Multidimensional en-face OCT imaging of the retina. Opt Express 17(5):4112–4133, pii: 177004

Sacchet D, Moreau J, Georges P, Dubois A (2008) Simultaneous dual-band ultra-high resolution full-field optical coherence tomography. Opt Express 16(24):19434–19446, pii: 174457

Sadda SR, Joeres S, Wu Z, Updike P, Romano P, Collins AT, Walsh AC (2007) Error correction and quantitative subanalysis of optical coherence tomography data using computer-assisted grading. Invest Ophthalmol Vis Sci 48(2):839–848. doi:10.1167/iovs.06-0554, pii: 48/2/839

Sano M, Shimoda Y, Hashimoto H, Kishi S (2009) Restored photoreceptor outer segment and visual recovery after macular hole closure. Am J Ophthalmol 147(2):313–318 e311. doi:10.1016/j.ajo.2008.08.002, pii: S0002-9394(08)00618-1

Sayanagi K, Sharma S, Yamamoto T, Kaiser PK (2009) Comparison of spectral-domain versus time-domain optical coherence tomography in management of age-related macular degeneration with ranibizumab. Ophthalmology 116(5):947–955. doi:10.1016/j.ophtha.2008.11.002, pii: S0161-6420(08)01143-3

Schepens CL (1947) A new ophthalmoscope demonstration. Trans Am Ophthalmol Soc 51:298–304

Shui YB, Holekamp NM, Kramer BC, Crowley JR, Wilkins MA, Chu F, Malone PE, Mangers SJ, Hou JH, Siegfried CJ, Beebe DC (2009) The gel state of the vitreous and ascorbate-dependent oxygen consumption: relationship to the etiology of nuclear cataracts. Arch Ophthalmol 127(4):475–482. doi:10.1001/archophthalmol.2008.621, pii: 127/4/475

Srinivasan VJ, Wojtkowski M, Witkin AJ, Duker JS, Ko TH, Carvalho M, Schuman JS, Kowalczyk A, Fujimoto JG (2006) High-definition and 3-dimensional imaging of macular pathologies with high-speed ultrahigh-resolution optical coherence tomography. Ophthalmology 113(11):2054 e2051–2014. doi:10.1016/j.ophtha.2006.05.046, pii: S0161-6420(06)00731-7

Srinivasan VJ, Adler DC, Chen Y, Gorczynska I, Huber R, Duker JS, Schuman JS, Fujimoto JG (2008) Ultrahigh-speed optical coherence tomography for three-dimensional and en face imaging of the retina and optic nerve head. Invest Ophthalmol Vis Sci 49(11):5103–5110. doi:10.1167/iovs.08-2127, pii: iovs.08-2127

Stefansson E (2006) Ocular oxygenation and the treatment of diabetic retinopathy. Surv Ophthalmol 51(4):364–380. doi:10.1016/j.survophthal.2006.04.005, pii: S0039-6257(06)00078-6

Stefansson E, Landers MB III, Wolbarsht ML (1982) Vitrectomy, lensectomy, and ocular oxygenation. Retina 2(3):159–166

Tao YK, Kennedy KM, Izatt JA (2009) Velocity-resolved 3D retinal microvessel imaging using single-pass flow imaging spectral domain optical coherence tomography. Opt Express 17(5):4177–4188, pii: 177008

Tappeiner C, Barthelmes D, Abegg MH, Wolf S, Fleischhauer JC (2008) Impact of optic media opacities and image compression on quantitative analysis of optical coherence tomography. Invest Ophthalmol Vis Sci 49(4):1609–1614. doi:10.1167/iovs.07-1264, pii: 49/4/1609

Wakabayashi T, Oshima Y, Fujimoto H, Murakami Y, Sakaguchi H, Kusaka S, Tano Y (2009) Foveal microstructure and visual acuity after retinal detachment repair: imaging analysis by Fourier-domain optical coherence tomography. Ophthalmology 116(3):519–528. doi:10.1016/j.ophtha.2008.10.001, pii: S0161-6420(08)01021-X

Wang RK, An L (2009) Doppler optical micro-angiography for volumetric imaging of vascular perfusion in vivo. Opt Express 17(11):8926–8940, pii: 179889

Williamson TH, Harris A (1994) Ocular blood flow measurement. Br J Ophthalmol 78(12):939–945

Winter M, Eberhardt W, Scholz C, Reichenbach A (2000) Failure of potassium siphoning by Muller cells: a new hypothesis of perfluorocarbon liquid-induced retinopathy. Invest Ophthalmol Vis Sci 41(1):256–261

Wolf-Schnurrbusch UE, Ceklic L, Brinkmann CK, Iliev ME, Frey M, Rothenbuehler SP, Enzmann V, Wolf S (2009) Macular thickness measurements in healthy eyes using six different optical coherence tomography instruments. Invest Ophthalmol Vis Sci 50(7):3432–3437. doi:10.1167/iovs.08-2970, pii: iovs.08-2970

Wong AD, Cooperberg PL, Ross WH, Araki DN (1991) Differentiation of detached retina and vitreous membrane with color flow Doppler. Radiology 178(2):429–431

Wu Z, Vazeen M, Varma R, Chopra V, Walsh AC, LaBree LD, Sadda SR (2007) Factors associated with variability in retinal nerve fiber layer thickness measurements obtained by optical coherence tomography. Ophthalmology 114(8):1505–1512. doi:10.1016/j.ophtha.2006.10.061, pii: S0161-6420(06)01600-9

Wu Z, Huang J, Dustin L, Sadda SR (2009) Signal strength is an important determinant of accuracy of nerve fiber layer thickness measurement by optical coherence tomography. J Glaucoma 18(3):213–216. doi:10.1097/IJG.0b013e31817eee20, pii: 00061198-200903000-00010

Xu J, Heys JJ, Barocas VH, Randolph TW (2000) Permeability and diffusion in vitreous humor: implications for drug delivery. Pharm Res 17(6):664–669

Yasuno Y, Miura M, Kawana K, Makita S, Sato M, Okamoto F, Yamanari M, Iwasaki T, Yatagai T, Oshika T (2009) Visualization of sub-retinal pigment epithelium morphologies of exudative macular diseases by high-penetration optical coherence tomography. Invest Ophthalmol Vis Sci 50(1):405–413. doi:10.1167/iovs.08-2272, pii: iovs.08-2272

Youm DJ, Kim JM, Park KH, Choi CY (2009) The effect of soft contact lenses during the measurement of retinal nerve fiber layer thickness using optical coherence tomography. Curr Eye Res 34(1):78–83. doi:10.1080/02713680802579188, pii: 908191255